A molecular dynamics study of a cascade induced irradiation creep mechanism in pure copper

Nargisse Khiara, Fabien Onimus, Jean-Paul Crocombette, Laurent Dupuy, Thomas Pardoen, Jean-Pierre Raskin, Yves Bréchet

N. Khiara, F. Onimus, J.-P. Crocombette, L. Dupuy, T. Pardoen, J-P. Raskin, Y. Bréchet (2022).
A molecular dynamics study of a cascade induced irradiation creep mechanism in pure copper,
Journal of Nuclear Materials, 541, 152336. DOI: 10.1016/j.jnucmat.2022.153518

A molecular dynamics study of a cascade induced irradiation creep mechanism in pure copper

Authors: Nargisse Khiara[1,5], Fabien Onimus[1], Jean-Paul Crocombette[2], Laurent Dupuy[2], Thomas Pardoen[3], Jean-Pierre Raskin[4], Yves Bréchet[1,5]

[1] Université Paris-Saclay, CEA, Service de Recherches Métallurgiques Appliquées, 91191, Gif-sur-Yvette, France
[2] Université Paris-Saclay, CEA, Service de Recherches de Métallurgie Physique, 91191, Gif-sur-Yvette, France
[3] Institute of Mechanics, Materials and Civil Engineering, UCLouvain, Place Sainte Barbe 2 L5.02.02, 1348, Louvain-la-Neuve, Belgium
[4] Institute of Information and Communication Technologies, Electronics and Applied Mathematics, UCLouvain, Place du Levant 2 L5.04.04, 1348, Louvain-la-Neuve, Belgium
[5] Science et Ingénierie des Matériaux et Procédés (SIMAP), Université Grenoble Alpes, 1130 rue de la Piscine BP 75, 38402, Saint Martin d'Hères, France

Abstract

Recently, *in-situ* TEM straining experiments on pure copper have unraveled a high stress irradiation creep mechanism. Irradiation induced unpinning of dislocations from defects has been observed and the mean pinning lifetime has been determined. In the present study, molecular dynamics simulations are performed on pure copper to investigate the impact of collision cascades on screw dislocations pinned on Frank loops under high-applied stresses at 300 K in order to further quantitatively elucidate this mechanism. The simulations indicate two possible dislocation unpinning mechanisms. Unpinning can occur through loop destruction when the cascade is generated on the pinning points of the dislocation (type 1 unpinning). Unpinning can also be triggered by the shear stresses building up around a cascade generated in front of the dislocation in the glide plane (type 2 unpinning). Type 2 unpinning generally leads to dislocation repinning on cascade residues, so that it should only marginally contribute to irradiation creep. The mean pinning lifetime due to type 1 unpinning in the conditions of the *in-situ* TEM experiments is derived from a simple model previously developed for zirconium, and is found in the same orders of magnitude as in the experiments.

Keywords: Irradiation creep, Copper, Molecular Dynamics, Collision cascade, Shock wave

Graphical Abstract

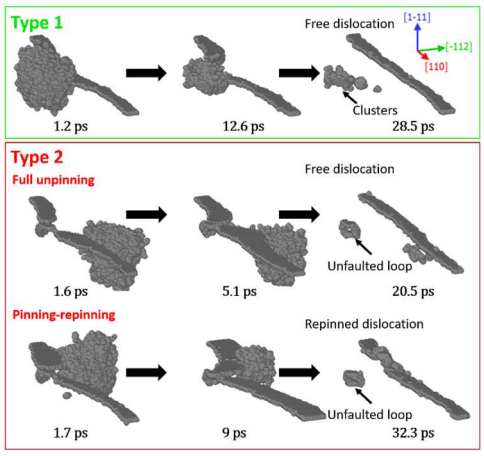

1. Introduction

Irradiation creep deformation is a visco-plastic deformation phenomenon occurring in components inside nuclear reactors at temperatures below $0.3T_m$ under applied load and irradiation. Irradiation creep has been mainly investigated through in-reactor experiments, allowing for the measurement of creep parameters and their dependence on neutron flux and fluence, temperature, stress, and material characteristics [1, 2, 3, 4]. However, such experiments are not amenable to the *in-situ* characterization of the elementary physical mechanisms at the origin of the macroscopic behavior. Therefore, although the macroscopic phenomenology for irradiation creep is relatively well rationalized, the underlying microscopic mechanisms are still unclear [5, 6]. Many theoretical mechanisms have been proposed in the literature, all involving atomic displacements and generation of point defects under irradiation, but differing in the detailed processes of their redistribution under applied stress [3, 5, 7, 8].

Very recently, a high stress irradiation creep phenomenon, first unraveled for a zirconium alloy was extended to pure copper which is considered as a model material for face-centered cubic (FCC) structures. Through *in-situ* transmission electron microscopy straining experiments under heavy ion irradiation, the authors [9, 10] observed an irradiation induced unpinning of dislocations from irradiation defects followed by dislocation glide. They proposed that the dislocation unpinning from irradiation defects is triggered by displacement cascades generated by irradiation. The mean pinning lifetime, i.e., the time necessary for a dislocation to unpin from an irradiation defect, was estimated around 25 and 40 seconds at room temperature for the zirconium alloy and pure copper, respectively.

Molecular dynamics (MD) is instrumental to investigate elementary mechanisms at the atomic level. MD simulations in copper related to the present context focused on dislocation interaction with defects [11, 12, 13, 14, 15] and cascade damage [16, 17]. The effect of displacement cascades on straight dislocations was studied for aluminum [18, 19], tungsten [20], Fe-20Cr-25Ni alloy [21], and Fe [22]. Some studies [18, 20, 21] evidenced that, when a cascade is generated on an edge dislocation, the dislocation can capture the generated point defects, leading to dislocation climb. For a screw dislocation, the dislocation can either capture point defects and form a helical turn, or, if subjected to loading, cross-slip [19, 21]. An intriguing cascade effect on dislocations was first observed by Fu et al. [20] in tungsten: when a cascade is generated near an edge dislocation, kinks are formed near the center of the cascade, and the dislocation glides toward the cascade. A similar phenomenon was observed by Heredia-Avalos et al. [22] in iron. The authors observed that a cascade generated near an edge dislocation dipole leads to the glide of the dislocations toward the cascade center. The authors reproduced the same phenomenon by generating a thermal spike near the dislocation dipole. Heredia-Avalos et al. [22] stated that the observed dislocation motion is triggered by the shock wave generated by the cascade (or the thermal spike). Starostenkov et al. [23] investigated the post cascade shock wave effect on a single edge dislocation or on an ensemble of edge dislocations in nickel, and the authors observed the glide of the dislocations toward the wave source. Korchuganov et al. [24, 25] found that a shock wave generated near an edge dislocation under applied stress in iron induces dislocation glide toward the wave source. The authors concluded that this phenomenon can contribute to irradiation creep.

In a previous study, we [26] investigated the effect of a cascade on a screw dislocation pinned on a loop at high applied stress in zirconium using MD simulations to reproduce similar configurations as in the TEM *in-situ* straining experiments of Gaumé et al. [9] on a zirconium alloy. A possible unpinning of dislocations by cascades was predicted at high stress levels slightly inferior to the critical stress for unpinning (without a cascade). In these simulations, the generated cascades had to encompass the pinning points of dislocations to induce unpinning, and we developed a simple closed-form model to

account for this phenomenon. Based on this closed-form model, we [26] estimated the mean pinning lifetime in the conditions of the experiments of Gaumé et al. [9] and obtained pinning lifetimes at high stress levels in the same orders of magnitude as the experimental pinning lifetime.

The objective of this work is to extend the numerical study using MD simulations made for zirconium to pure copper and to compare the MD results to our recently published experimental results on pure copper [10].

2. MD simulation method

2.1. Interaction dislocation / loop

All the molecular dynamics simulations are performed on pure copper (FCC structure) using the Large-scale Atomic and Molecular Massively Parallel Simulator (LAMMPS) [27]. The embedded atom method (EAM) used is a potential derived and updated by Ackland et al. [28] to take into account close-range repulsion for irradiation studies (Cu1_v2). Interactions between screw dislocations and irradiation defects were observed during our previous *in-situ* straining experiments [10]. The objective is to reproduce a similar configuration as in the experiments. The X, Y, and Z axis of the simulation box correspond respectively to the directions $[110]$, $[\bar{1}12]$ and $[1\bar{1}1]$. The box dimensions are approximatively $400\,\text{Å} \times 234\,\text{Å} \times 220\,\text{Å}$, along the X, Y and Z directions respectively, which corresponds to around 1.6 million atoms. The simulation box dimension along the X axis is close to the mean obstacle spacing in our *in-situ* straining experiments under irradiation [10] (estimated between 45 and 70 nm). Periodic boundaries are applied in the X and Y directions.

The methodology is similar to the one used for zirconium in our previous MD study [26]. First, a molecular dynamics simulation box containing a screw dislocation and a Frank loop is generated using NUMODIS [29, 30, 31]. NUMODIS is a Dislocation Dynamics simulation code, but has recently incorporated a tool to generate simultaneously MD and DD identical simulation boxes to perform similar MD and DD simulations.

The screw dislocation has a Burgers vector $\boldsymbol{b} = \frac{1}{\sqrt{2}}[110]$, and a glide plane $(1\bar{1}1)$. The Frank loop has a $(\bar{1}\bar{1}\bar{1})$ habit plane and contains 61 SIAS (self-interstitial atoms), which corresponds to an approximate loop diameter of 2.3 nm. The loop dimension properly compares to the 2 nm loops observed in our experiments [10]. The Frank loop center lies in the dislocation glide plane. As for the previous MD study on zirconium, this specific configuration is chosen since the interaction of the chosen dislocation and Frank loop leads to the formation of a helical turn (Figure 1.c), which is the configuration for which the obstacle is the strongest [13].

The simulation box is first thermally equilibrated at 300 K for 50 ps with a time-step of 5 fs. The crystal is then divided into three layers along the Z direction. The atoms of the top and bottom layers are held in fixed positions with respect to one another, while no constraint is imposed on the atoms of the middle layer. As presented in Figure 1.a.1, a shear strain rate of 10^{-6} ps^{-1} is applied on the atoms of the top layer (in green), while the atoms of the bottom layer are held in fixed positions (in grey). The corresponding shear stress is derived from the force applied by the free atoms of the middle layer on the upper layer atoms. The shear stress evolution with strain is presented in Figure 1.b. In order to smooth out stress fluctuations (blue curve), an averaging over 1000 time-steps is performed (red curve), corresponding to a duration of 250 ps and a strain increment of 0.025%. The critical stress τ_c for dislocation unpinning is the shear stress necessary for the release of the dislocation (without cascade) and is equal to 200 MPa.

The processing and visualization tool OVITO [32] is used to analyze and post-process the MD results. The common neighbor analysis tool (CNA) [33] is used to display atoms that are not in perfect FCC positions, whereas the dislocation extraction algorithm (DXA) [34] is used to display dislocations. The Voronoi analysis method is used to calculate the atomic volume with OVITO [32, 35]. This allows calculating the atomic stresses in units of pressure from LAMMPS atomic stress outputs.

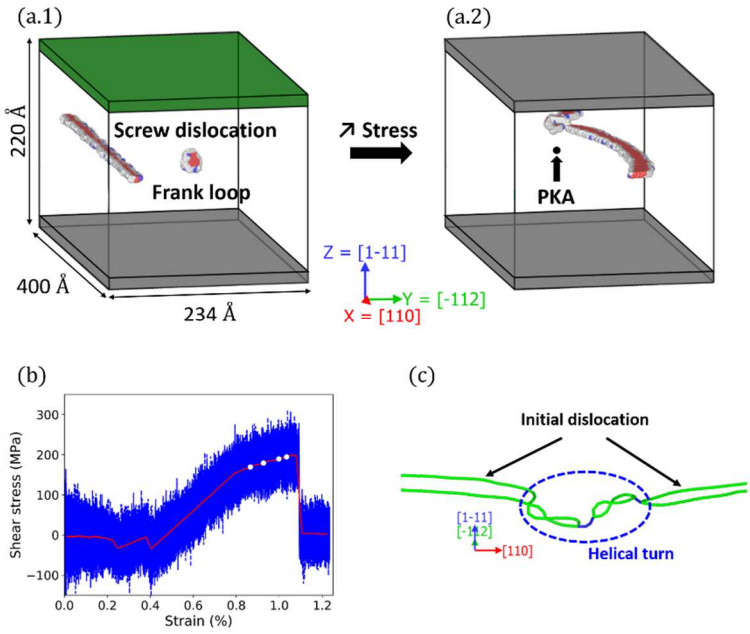

Figure 1 – Boundary conditions (using the CNA method): (a.1) for the interaction of the dislocation with the loops – (a.2) for the cascade calculations – (b) Stress-strain curve for the interaction dislocation loop (without cascade) before (blue) and after (red) curve smoothing, the white points represent the shear stresses investigated: $0.85\tau_c$, $0.9\tau_c$, $0.95\tau_c$ *and* $0.975\tau_c$ *– (c) Helical turn displayed using the DXA algorithm.*

2.2. Cascade effect on pinned dislocation

In order to investigate the effect of a cascade on a screw dislocation pinned on a Frank loop for stresses slightly inferior to the critical stress for unpinning, the same methodology as the one proposed for zirconium is used [26]. Four high stress levels below the critical stress are selected: $0.85\tau_c$, $0.9\tau_c$, $0.95\tau_c$ and $0.975\tau_c$ (white points in Figure 1.b). The atomic configurations corresponding to the selected shear stresses are extracted (Figure 1.a.2). After a thermal equilibration at 300 K for 50 ps with a time-step of 5 fs, the atoms of the top and bottom layers are held fixed (in grey in Figure 1.a.2), so that the total strain is kept constant. To generate a displacement cascade, an energy (between 10 and 30 keV) along the $+Z$ direction is transferred to an atom, called Primary Knock-on-Atom (PKA). Since the PKA velocity direction is along the $+Z$ direction, the center of the cascade generated lies over the PKA initial position along the $+Z$ axis. A variable time step is defined in order to limit the distance traveled by atoms to less than 1% of the lattice constant. The simulations are run for 150 000 time-steps, corresponding to approximately 100 ps, which is long enough to ensure that ballistic and thermally enhanced recovery stages of the cascade are over. The temperature is set at 300 K in order to allow for comparisons with our in-situ experiments performed at room temperature [10].

In this study, the impact of the shear stress level, PKA position, and energy are investigated. Since various configurations are studied, the PKA positions and energies selected for each configuration will be detailed in the following sections.

3. Results

3.1. Impact of the PKA position

The unpinning of screw dislocations from Frank loops is predicted in the two different configurations presented in Figure 2. The first configuration, called type 1 unpinning, is similar to the one we observed for zirconium [26]. In this case, the cascade encompasses the helical turn. After the end of the cascade, the dislocation is free and the loop is destroyed. Residual clusters are formed behind the dislocation. Unlike in zirconium for which the loop is only partially destroyed, the Frank loop in copper is completely destroyed [26].

The second configuration that induces dislocation unpinning from the loop, called type 2 unpinning, occurs for cascades generated in front of the dislocation along the glide direction. As shown in Figure 2, when the cascade peak occurs, the cascade starts to attract one or both segments of the dislocation. The dislocation segments enter in contact with the displaced atoms within the cascade. The dislocation then unpins from the initial Frank loop, leaving the Frank loop unfaulted, as in the case of a standard dislocation unpinning from a Frank loop with increasing stress without cascade [13]. The dislocation is often repinned on residual clusters left after cascade relaxation and forms a helical turn (Figure 2), as observed by Voskoboinikov et al. [19] for displacement cascades generated near straight screw dislocations in aluminum. Type 2 unpinning is thus divided into two subcategories: unpinning-repinning mechanism (when dislocations unpin from loops but repin on cascade residues), and permanent unpinning (when dislocations remain straight and free to glide under stress). Permanent unpinning generally occurs when the cascade is generated slightly below the dislocation glide plane (Figure 2).

To ensure that the two unpinning types do not result from box size effects, calculations were repeated for a larger simulation box size along the Y axis (405 Å rather than 234 Å), and both unpinning types, with similar trends, were captured for the larger box in comparison with the smaller box. More details on this analysis can be found in Supplementary Data. Likewise, we checked using various PKA directions that both unpinning can occur when PKA initial velocity is along axes other than the $+Z$ axis.

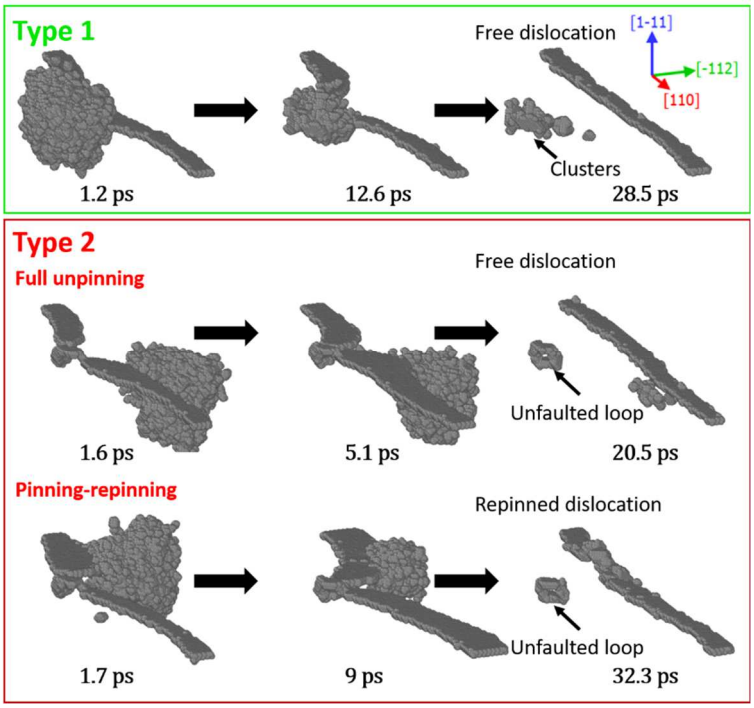

Figure 2 – Snapshots showing the time evolution of core atoms (using the CNA method) in a case where type 1 and type 2 unpinning processes of the dislocation are triggered for 20 keV cascades (the corresponding videos can be found in the Supplementary data).

3.2. Impact of stress

The impact of the stress level on the unpinning probability is investigated at different PKA positions. As stated earlier, four stress levels are studied: $0.85\tau_c$, $0.9\tau_c$, $0.95\tau_c$ and $0.975\tau_c$. A PKA position grid around the dislocation is addressed. For $0.85\tau_c$ and $0.9\tau_c$, the grid is of $160\ \text{Å} \times 160\ \text{Å} \times 160\ \text{Å}$, with a spacing between PKA positions of $20\ \text{Å}$. For $0.95\tau_c$ and $0.975\tau_c$, a grid of $160\ \text{Å} \times 220\ \text{Å} \times 160\ \text{Å}$ is selected with a spacing between PKAs of $20\ \text{Å}$. The PKA energy is set at 20 keV and the PKA direction is always along the $+Z$ axis.

The grids and simulation results are presented in Figure 3: the small blue points represent the PKA positions that did not induce unpinning, the green and red points represent PKA that triggered type 1 and type 2 unpinning, respectively. Increasing unpinning frequency with increasing stress is observed. Type 1 unpinning prevails at lower stresses ($0.85\tau_c$ and $0.9\tau_c$,) and type 2 unpinning prevail at higher stresses ($0.95\tau_c$ and $0.975\tau_c$). This dependency on the sensitivity to stress is more important for type 2 unpinning. Moreover, the repinning probability is around $94\%(\pm 4\%)$ at $0.95\tau_c$ and around $80\%(\pm 4\%)$ at $0.975\tau_c$. Therefore, it appears that type 2 permanent unpinning probability increases with stress.

To better visualize the PKA position effect on unpinning, the unpinning probability at both $0.95\tau_c$ and at $0.975\tau_c$ projected along the X, Y and Z directions are represented in Figure 4 and Figure 5, respectively. For type 1 unpinning, over the X and Y directions, the maximum unpinning probability is centered on the helical turn. For type 2 unpinning, over the Y direction, the unpinning probability is at its maximum around $50 - 60\ \text{Å}$ in front the mean dislocation position along the Y axis. Over the X direction, the maximum probability is around the helical turn, but with a wider spread in comparison with type 1 unpinning. The wider spread for type 2 unpinning along the X axis can be explained by the fact that the cascade can trigger dislocation unpinning by only attracting one of the segments of the dislocation. Over the Z axis, the maximum unpinning probability is observed approximatively at the

same position for both unpinning types. The maximum is observed under the dislocation along the Z axis, since the PKAs at these positions generate cascades approximately on the dislocation glide plane.

To summarize, type 1 unpinning occurs when the cascade is on the helical turn, whereas type 2 unpinning takes place when the cascade is generated in front of the dislocation in the glide plane.

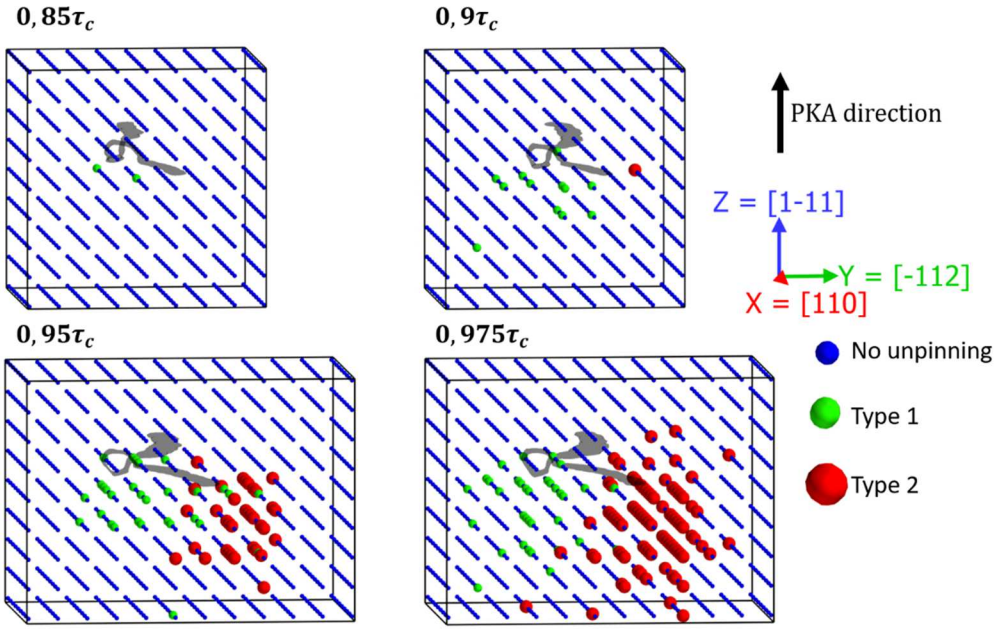

Figure 3 – MD simulation results for four stress levels for a PKA energy $E_{PKA} = 20\ keV$ showing the dislocation in grey, the "inefficient" PKAs in blue and the "efficient" type 1 PKAs in green and type 2 in red.

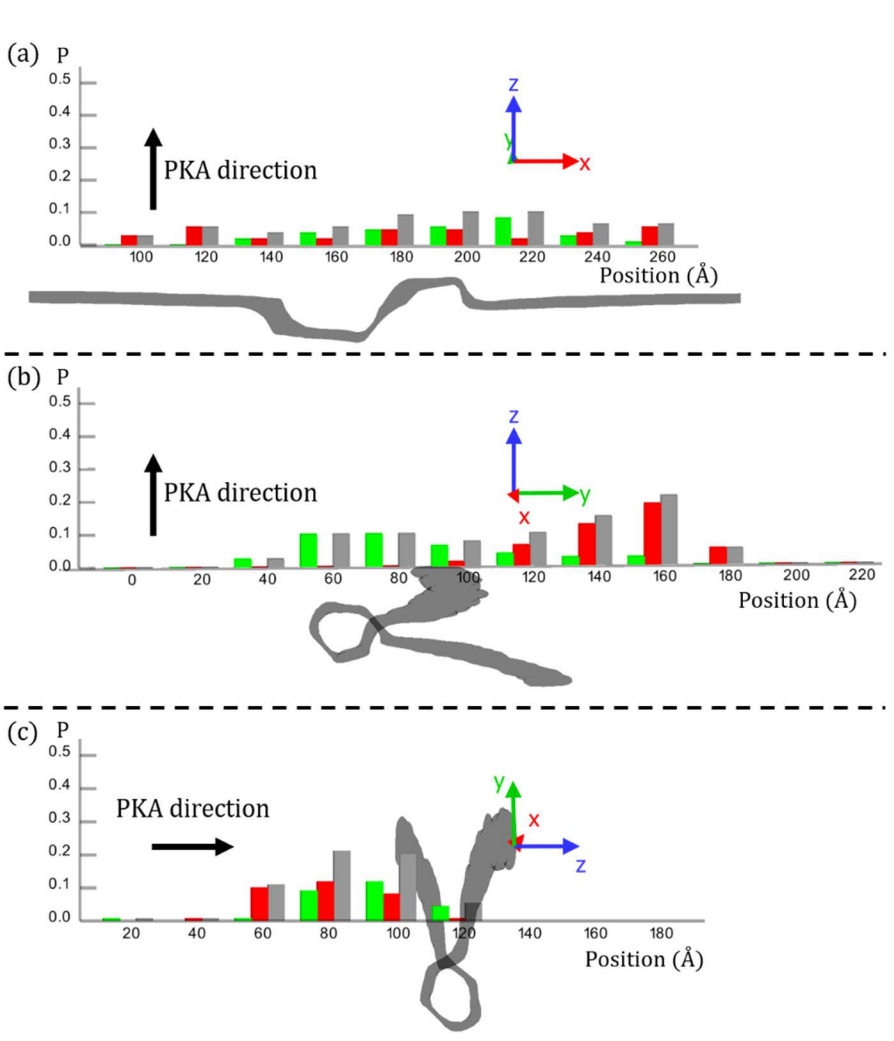

Figure 4 – Unpinning probability for a shear stress $\tau = 0.95\tau_c$ as a function of the position of the PKA (a) along the X axis $[110]$; (b) along the Y axis $[\bar{1}12]$; (c) along the Z axis $[1\bar{1}1]$. Type 1, type 2, and total unpinning probabilities are represented in green, red, and grey, respectively.

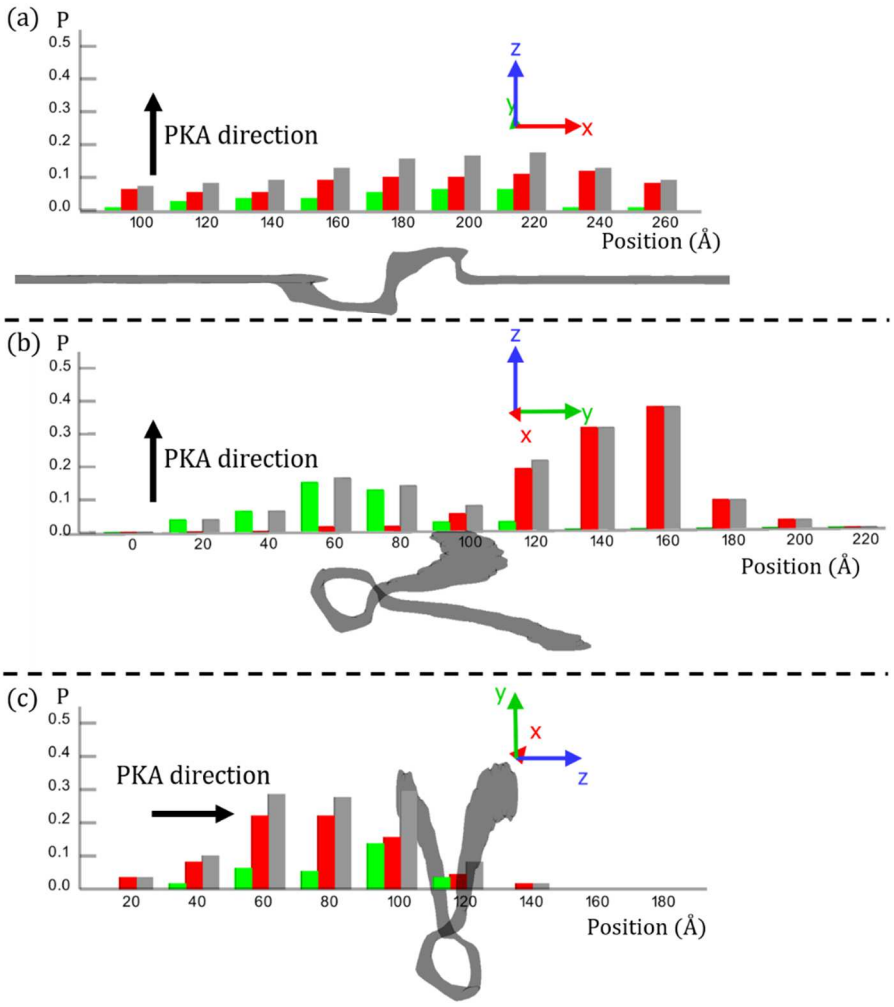

Figure 5 – Unpinning probability for a shear stress $\tau = 0.975\tau_c$ as a function of the position of the PKA (a) along the X axis $[110]$; (b) along the Y axis $[\bar{1}12]$; (c) along the Z axis $[1\bar{1}1]$. Type 1, type 2, and total unpinning probabilities are represented in green, red, and grey, respectively.

3.3. Impact of PKA energy

The impact of the PKA energy is investigated at a selected stress level of $0.95\tau_c$. Four PKA energies are investigated: 10 keV, 15 keV, 20 keV, and 30 keV. The PKA position grid investigated is of 160 Å $\times$ 160 Å $\times$ 160 Å with a spacing between PKA positions of 40 Å. The PKA velocity direction is always along the $+Z$ axis. The PKA position grid and simulation results are presented in Figure 6. Increasing unpinning probability is observed with increasing PKA energy. The sensitivity to the PKA energy seems higher for type 2 unpinning. The repinning probability is equal to 100% at 10 keV, 83% at 15 keV, 86% at 20 keV and 80% at 30 keV. There are, however, large uncertainties on these values since there is only 1 effective type 2 unpinning at 10 keV, 6 at 15 keV, 7 at 20 keV, and 10 at 30 keV. Therefore, more investigation is needed to draw any conclusions on the effect of the PKA energy on the repining probability.

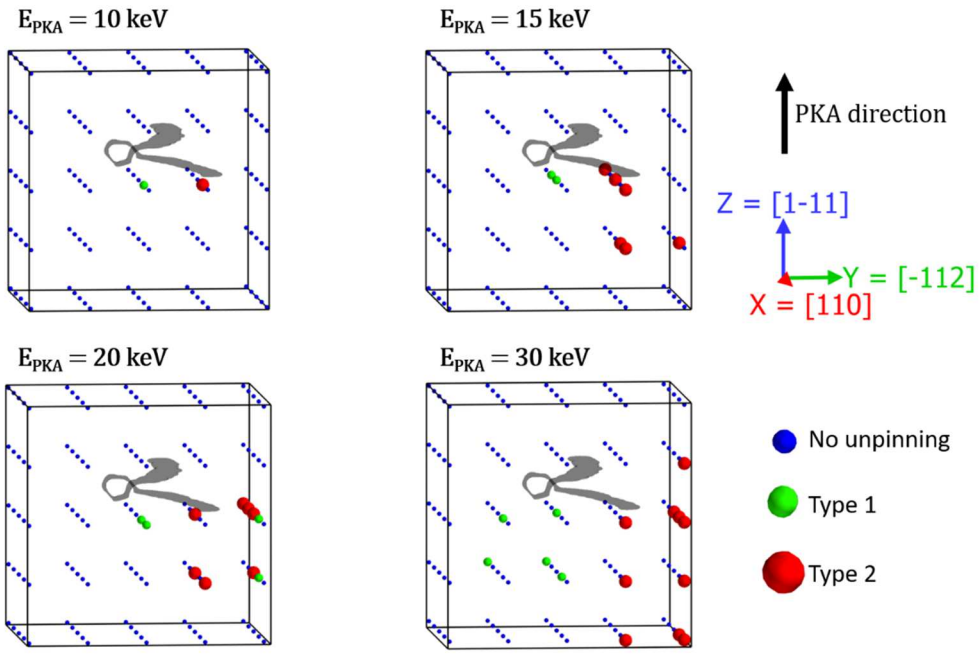

Figure 6 – MD simulation results for four PKA energies at a shear stress level $\tau = 0.95\tau_c$ showing the dislocation in grey, the "inefficient" PKAs in blue, and the "efficient" type 1 PKA in green and type 2 in red.

4. Discussion

4.1. Type 2 unpinning

Type 2 unpinning occurs for cascades generated in front of the dislocation along the glide direction through a process similar to an increase in stress, with an unfaulted loop left after the unpinning process. When the cascade peak occurs, one or both segments of the dislocation glide toward the cascade center and enter in contact with the displaced atoms within the cascade. The dislocation then unpins from the Frank loop.

Type 2 unpinning resembles behavior seen in previous work on cascade, thermal spike, and shock wave effects on straight dislocations. The dislocation motion triggered by a cascade (or a shock wave) toward the cascade center (or the wave source) was reported by several authors for different metals through MD simulations [20, 22, 25, 24, 23]. Cascade induced glide of dislocations was also theoretically investigated by Trinkaus [36] and Zhukov and Boldin [37].

Heredia-Avalos [22] attributed the initial dislocation motion toward the displacement cascade to the shock wave generated by the cascade. The same observation is made in our MD simulations. Figure 7 shows frames representing the initial dislocation motion during type 2 unpinning, along with the atomic pressure and shear stress fields. A correlation is observed between the dislocation motion and the time of arrival of the shear stress shock wave (and the pressure shock wave) at the dislocation. As reported by Béland et al. [35] , the shock wave appears during the sonic step of the cascade, and propagates during the sonic and thermal annealing steps. As shown in Figure 7, the dislocation starts its first motion when the shock wave arrives near the dislocation. There is also a correlation between the first dislocation motion and the sign of the shear stress wave. At a time of about 1.21 ps and 1.78 ps in Figure 7, the right segment moves significantly toward the cascade center whereas the left segment moves slightly backward. This can be simply linked to the signs of the shear stresses and to the resultant Peach-Köhler force.

Far from the dislocation, the same shear stress distribution as in perfect crystal is observed: negative shear stress in the upper right and positive shear stress in the upper left (Figure 7). Near the dislocation,

the negative shear stress wave is either attenuated or absent (Figure 7) in comparison with a perfect crystal (see supplementary data for more examples). Therefore, in the area of negative shear stress, the dislocation can either partially and slightly move backward (Figure 7) or is unaffected. On the contrary, in the positive shear stress area, the dislocation is highly affected by the stress shock wave and partially glides toward the center of the cascade.

The maximum unpinning probability is found for initial PKA positions at about $50 - 60$ Å from the mean dislocation position along the Y axis. This can easily be explained in terms of cascade radius (Figure 4 and Figure 5). Indeed, the shear stresses are generated around the cascade core, which, at its peak, has a radius of $40 - 50$ Å for 20 keV cascades.

Type 2 unpinning probability increases with increasing PKA energy and increasing stress. This is analogous to the observations of Korchuganov et al. [24] for straight edge dislocations under applied shear stress and exposed to a shock wave in iron. The authors observed that the larger the shear stress and the amplitude of the shock wave, the larger the displacement of the dislocation.

One of the main objectives of this work is to estimate, based on the MD calculations, the mean pinning lifetime in the experimental conditions of Ref. [10]. After dislocation unpinning from the Frank loop, there are two possible outcomes: the dislocation is either repinned (unpinning-repinning process) or completely free (permanent unpinning process). Type 2 unpinning appears and becomes predominant at very high stress level. However, there is a very high repinning probability on cascade residues. For 20 keV cascades, up to a stress level of $0.95\tau_c$, permanent type 2 unpinning represents less than 7% of type 1 unpinning and is therefore negligible.

For $0.975\tau_c$, type 2 permanent unpinning induces an increase in the unpinning probability of nearly 50%. Therefore, except for very high stress levels, type 2 permanent unpinning is negligible in comparison with type 1 unpinning. Moreover, in Ref. [10], the dislocation mean free path after unpinning is estimated at around 45 nm, which is not compatible with type 2 unpinning-repinning mechanism. Indeed, the mean dislocation glide distance before repinning is around 0.7 and 0.6 nm with a maximum traveled distance of 7 and 8 nm at respectively $0.95\tau_c$ and $0.975\tau_c$, which is way below the experimental dislocation free path.

Another possible effect of type 2 unpinning on irradiation creep can arise from the potential lower obstacle strength of cascade residues in comparison with the initial Frank loop. In order to investigate this effect, 25 post-cascade MD straining calculations are performed on configurations for which type 2 unpinning-repinning process was triggered by a 20 keV cascade. The post unpinning-repinning critical stress is found at around 93% of the initial critical stress. More details on this analysis can be found in supplementary data. This shows that type 2 unpinning-repinning might be equivalent to a very slight reduction in obstacle strength. However, there is a wide spread of critical stress over and under the initial critical stress. Therefore, more investigations on this subject, especially on the effect of loop size and PKA energy, are needed to draw any definitive conclusion.

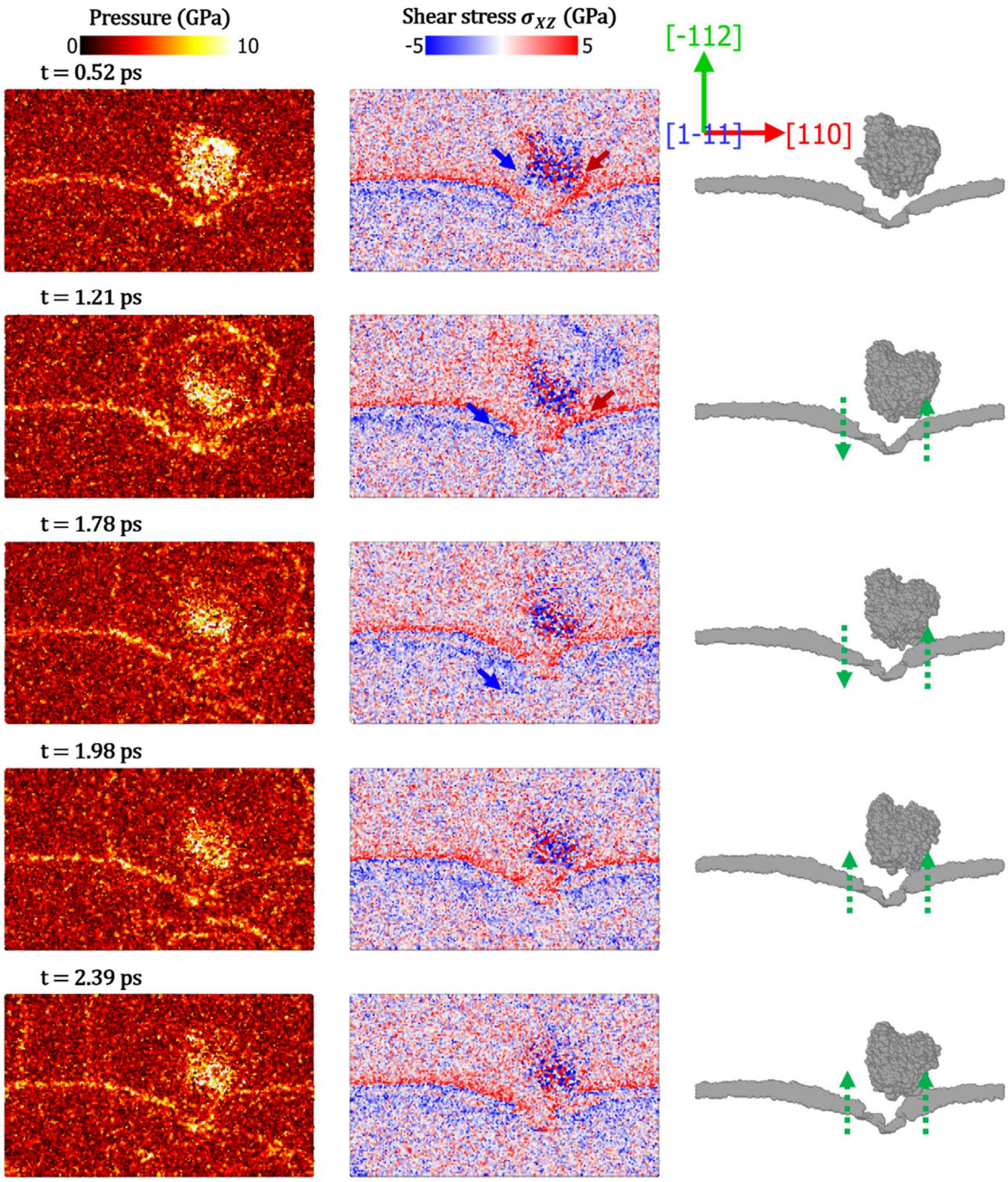

Figure 7 – Atoms colored by pressure and shear stress on the left and in the middle, and display of irregular atoms using the CNA tool on the right at different times after PKA creation. The corresponding videos can be found in the Supplementary data.

4.2. Type 1 unpinning

The type 1 unpinning process is driven by the destruction of the loop. Following the conclusions of the previous analysis on type 2 unpinning, type 1 unpinning has a predominant effect on irradiation creep, at least up to $0.95\tau_c$.

Based on the MD calculations, the unpinning probability and standard deviation are defined as follows:

$$P = {N_{type\ 1}}/{N_{tot}}\ , \tag{1}$$

$$SE = \sqrt{{P(1-P)}/{N_{tot}}}\ . \tag{2}$$

where $N_{type\ 1}$ is the number of effective type 1 PKAs and N_{tot} is the number of investigated points.

From the unpinning probability, an effective volume and the corresponding standard deviation can be defined through:

$$V_{eff} = P \times V_{tot}\ , \tag{3}$$

$$SE_{V_{eff}} = SE \times V_{tot}\ . \tag{4}$$

As stated earlier, type 1 unpinning is triggered when the cascade encompasses the helical turn. In order to take this observation into account, we proposed a simple model to calculate the effective volume for zirconium: if a cascade with a radius R_c, that depends on the PKA energy, encompasses the pinning points of the dislocation, type 1 dislocation unpinning occurs. The distance between pinning points Δ^{loop} depends on stress. The higher the stress, the lower this distance.

Therefore, the effective volume can be simply calculated as [26]:

if $R_c(E_{PKA}) < \frac{\Delta^{loop}(\tau)}{2}$

$$V_{eff}(E_{PKA}, \tau) = 0\ , \tag{5}$$

if $R_c(E_{PKA}) > \frac{\Delta^{loop}(\tau)}{2}$

$$V_{eff}(E_{PKA}, \tau) = \frac{\pi}{12}\left(4R_c(E_{PKA}) + \Delta^{loop}(\tau)\right)\left(2R_c(E_{PKA}) - \Delta^{loop}(\tau)\right)^2\ . \tag{6}$$

As in Ref. [26], to calculate cascade radius for a given PKA energy, 10000 cascade calculations are performed using Iradina [38, 39] for the investigated PKA energy (here 20 keV). Moreover, the pinning point spacing positions is taken to be the distance between the upper and the bottom parts of the loop (as shown by the insert in Figure 8.a).

Figure 8.a represents the evolution of the effective volume with stress for 20 keV cascades based on the MD calculations (in green) and on the simple model developed in Ref. [26] (in red). The error bars for the model come from the dispersion in cascade radii. The model seems to be in good agreement with MD calculations, although a slight underestimation is observed.

Based on the hypothesis that the effective volume around dislocation pinning points for a given stress and PKA energy can be derived from Eq. 5 and 6, we [26] developed a closed-form model to estimate the mean pinning lifetime evolution with stress. This model accounts for cascade fragmentation into subcascades. For copper, the threshold energy for cascade fragmentation into subcascades is found to be around 60 keV [40].

Following the model developed before, the evolution of the pinning lifetime with stress in the experimental conditions of the *in-situ* straining experiments under irradiation in Ref. [10] is represented in Figure 8.b. At high stress levels, the pinning lifetimes are in the same ranges as the experimental value we obtained [10]. Therefore, the proposed cascade induced unpinning mechanism can provide an explanation to the irradiation triggered unpinning of dislocations at high stress levels (over $0.8\tau_c$) observed experimentally. Moreover, the minimum stress for cascade induced unpinning can also be derived from this model. This minimum stress is found equal to $0.76\tau_c$ and corresponds to the stress level for which the condition $R_c(E_{PKA}) < \frac{\Delta^{loop}(\tau)}{2}$ is valid for the largest possible cascades (60 keV cascades given the threshold energy for cascade fragmentation).

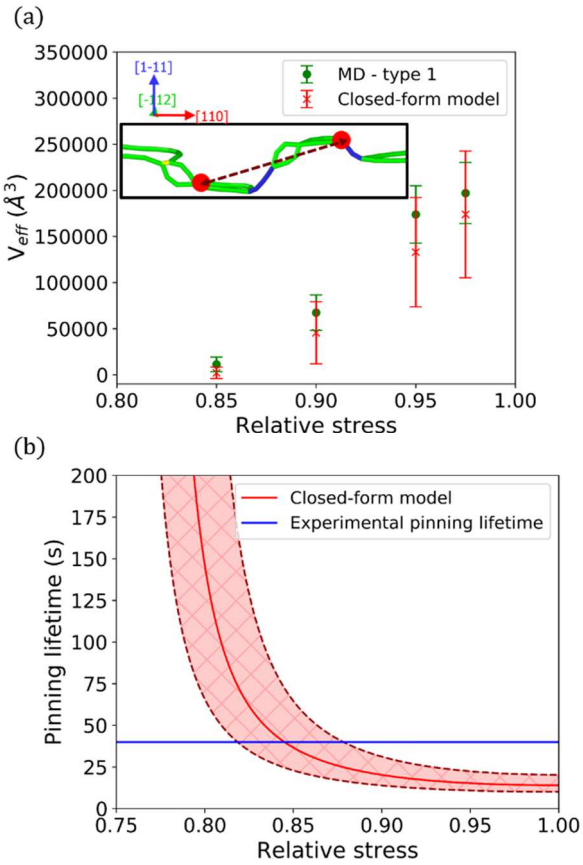

Figure 8 – (a) Evolution of the effective volume with stress, the insert shows the dislocation using the DXA algorithm with the pinning points considered in red – (b) Pinning lifetime evolution with stress based on the distance between the pinning points in red (solid line), the hatched areas between the dashed lines represent the standard deviation, the blue line represents the experimental value obtained in Ref. [10].

5. Conclusion

MD simulations are performed on pure copper, considered as a model material for FCC metals, in order to investigate the possible unpinning by a displacement cascade of a screw dislocation pinned on a Frank loop and provide new insights on high stress irradiation creep mechanisms.

The main findings of this work are the following.

- The possible unpinning of screw dislocations pinned on a Frank loop occurs at high stress levels (at least starting from $0.85\tau_c$);
- Two unpinning processes are observed: type 1 and type 2 unpinning;
- Type 1 unpinning is similar to the one we have previously unraveled for zirconium [26]: the cascade occurs on the helical turn and induces the destruction of the loop, leaving a free dislocation.
- Type 2 unpinning is triggered by the shear stresses generated around the cascade core. The dislocation unpins from the loop as in the case of an increase in shear stress: the loop is left unfaulted. In a large majority of cases, the dislocation is very often pinned on cascade residues (unpinning-repinning process). In very few cases, the dislocation is free (permanent unpinning process);
- Type 2 unpinning occurs and becomes dominant at very high stress levels (> $0.95\tau_c$);
- Both unpinning types are more likely to occur with increasing stress and increasing PKA energy;

- Since type 2 unpinning is observed at very high stress levels and leads in the majority of cases to dislocation repinning, its impact on irradiation creep is most likely far smaller than type 1 unpinning;
- The model we developed previously for zirconium [26] is applied to reproduce type 1 unpinning: if the cascade encompasses the helical turn, the dislocation unpins. This model slightly underestimates the unpinning probability but gives values in the same orders as the ones obtained from the MD calculations. Using this simple model, the mean pinning lifetime of dislocations is derived and values similar to the experimental pinning lifetime estimated in Ref. [10] are obtained. Therefore, this cascade induced unpinning of dislocation process may provide an explanation for the high stress irradiation creep phenomenon observed during *in-situ* experiments.

6. Acknowledgment

This work was granted access to the HPC resources of TGCC under the allocations 2019-A0070911020 and 2020-A0090911020 made by GENCI.

7. References

[1] E. S. Aitkhozhin and E. V. Chumakov, "Radiation-induced creep of copper, aluminium and their alloys," *Journal of nuclear materials,* vol. 233, pp. 537-541, 1996.

[2] J. Garnier, Y. Bréchet, M. Delnondedieu, C. Pokor, P. Dubuisson, A. Renault, X. Averty and J. P. Massoud, "Irradiation creep of SA 304L and CW 316 stainless steels: Mechanical behaviour and microstructural aspects. Part I: Experimental results," *Journal of nuclear materials,* vol. 413, no. 2, pp. 63-69, 2011.

[3] F. Onimus, T. Jourdan, C. Xu, A. Campbell and M. Griffiths, "Irradiation Creep in Materials," in *Comprehensive Nuclear Materials (Second Edition)*, vol. 1, 2020, pp. 310-366.

[4] B. N. Singh, D. J. Edwards, S. Tähtinen, P. Moilanen, P. Jacquet and J. Dekeyser, "Final report on in-reactor tensile tests on OFHC-Copper and CuCrZr alloys.," 2004.

[5] J. R. Matthews and M. W. Finnis, "Irradiation creep models—An overview," *Journal of Nuclear Materials,* vol. 159, pp. 257-285, 1988.

[6] F. A. Garner and D. S. Gelles, "Irradiation creep mechanisms: an experimental perspective," *Journal of Nuclear Materials,* vol. 159, no. 286-309, 1988.

[7] W. G. Wolfer, "Correlation of radiation creep theory with experimental evidence.," *Journal of Nuclear Materials,* vol. 90, no. 1-3, pp. 175-192, 1980.

[8] L. K. Mansur and T. C. Reiley, "Irradiation creep by dislocation glide enabled by preferred absorption of point defects—theory and experiment.," *Journal of Nuclear Materials,* vol. 90, no. 1-3, pp. 60-67, 1980.

[9] M. Gaumé, P. Baldo, F. Mompiou and F. Onimus, "In-situ observation of an irradiation creep deformation mechanism in zirconium alloys," *Scripta Materialia,* vol. 154, pp. 87-91, 2018.

[10] N. Khiara, F. Onimus, S. Jublot-Leclerc, T. Jourdan, T. Pardoen, J.-P. Raskin and Y. Bréchet, "In-situ TEM irradiation creep experiment revealing radiation induced dislocation glide in pure copper," *Acta Materialia,* p. 117096, 2021.

[11] M. Doyama, Y. Kogure and T. Nozaki, "Interactions between point defects and edge dislocations in copper.," *Nuclear Instruments and Methods in Physics Research Section B: Beam Interactions with Materials and Atoms,* vol. 255, no. 1, pp. 85-91, 2007.

[12] H. J. Lee, J. H. Shim and B. D. Wirth, "Molecular dynamics simulation of screw dislocation interaction with stacking fault tetrahedron in face-centered cubic Cu.," *Journal of Materials Research,* vol. 22, no. 10, pp. 2758-2769, 2007.

[13] T. Nogaret, C. Robertson and D. Rodney, "Atomic-scale plasticity in the presence of Frank loops," *Philosophical Magazine,* vol. 87, no. 6, pp. 945-966, 2007.

[14] Y. N. Osetsky, D. Rodney and D. J. Bacon, "Atomic-scale study of dislocation–stacking fault tetrahedron interactions. Part I: mechanisms.," *Philosophical Magazine,* vol. 86, no. 16, pp. 2295-2313, 2006.

[15] D. Rodney, "Molecular dynamics simulation of screw dislocations interacting with interstitial frank loops in a model FCC crystal.," *Acta Materialia,* vol. 52, no. 3, pp. 607-614, 2004.

[16] A. F. Calder, D. J. Bacon, A. V. Barashev and Y. N. Osetsky, "On the origin of large interstitial clusters in displacement cascades.," *Philosophical Magazine,* vol. 90, no. 7-8, pp. 863-884, 2010.

[17] T. D. De la Rubia and W. J. Phythian, "Molecular dynamics studies of defect production and clustering in energetic displacement cascades in copper.," *Journal of nuclear materials,* vol. 191, pp. 108-115, 1992.

[18] R. E. Voskoboinikov, "Interaction of collision cascades with an isolated edge dislocation in aluminium.," *Nuclear Instruments and Methods in Physics Research Section B: Beam Interactions with Materials and Atoms,* vol. 303, pp. 125-128, 2013.

[19] R. E. Voskoboinikov, "MD simulations of collision cascades in the vicinity of a screw dislocation in aluminium.," *Nuclear Instruments and Methods in Physics Research Section B: Beam Interactions with Materials and Atoms,* vol. 303, pp. 104-107, 2013.

[20] B. Fu, S. Fitzgerald, Q. Hou, J. Wang and M. Li, "Effect of collision cascades on dislocations in tungsten: A molecular dynamics study.," *Nuclear Instruments and Methods in Physics Research Section B: Beam Interactions with Materials and Atoms,* vol. 393, pp. 169-173, 2017.

[21] Z. Lu, L. Xu, T. Chen, L. Tan and H. Xu, "Interactions between displacement cascade and dislocation and their influences on Peierls stress in Fe-20Cr-25Ni alloys.," *Computational Materials Science,* vol. 160, pp. 279-286, 2019.

[22] S. Heredia-Avalos, C. Denton, J. Moreno-Marín, E. Martinez and M. Caturla, "Collision cascade effects near an edge dislocation dipole in alpha-Fe: Induced dislocation mobility and enhanced defect clustering.," *Journal of Nuclear Materials,* vol. 543, p. 152459, 2021.

[23] M. D. Starostenkov, A. I. Potekaev, A. V. Markidonov, V. V. Kulagina and L. S. Grinkevich, "Dynamics of edge dislocations in a low-stability FCC-system irradiated by high-energy particles.," *Russian Physics Journal,* vol. 59, no. 9, pp. 1446-1453, 2017.

[24] A. Korchuganov, K. Zolnikov, D. Kryzhevich, V. Chernov and S. Psakhie, "Mobility of edge dislocations in stressed iron crystals during irradiation.," *AIP Conference Proceedings, AIP Publishing LLC,* vol. 1683, no. 1, p. 020095, 2015.

[25] A. V. Korchuganov, V. M. Chernov, K. P. Zolnikov, D. S. Kryzhevich and S. G. Psakhie, "MD simulation of primary radiation damage in metals with internal structure.," *Inorganic Materials: Applied Research,* vol. 7, no. 5, pp. 648-657, 2016.

[26] N. Khiara, F. Onimus, L. Dupuy, W. Kassem, J. Crocombette, T. Pardoen, J. Raskin and Y. Bréchet, "A novel displacement cascade driven irradiation creep mechanism in α-zirconium: A molecular dynamics study.," *Journal of Nuclear Materials,* p. 152336, 2020.

[27] S. Plimpton, "Fast Parallel Algorithms for Short-Range Molecular Dynamics," *Journal of Computational Physics,* vol. 117, no. http://lammps.sandia.gov, pp. 1-19, 1995.

[28] G. Ackland, G. Tichy, V. Vitek and M. Finnis, "Simple N-body potentials for the noble metals and nickel," *Philosophical Magazine A,* vol. 56, no. 6, pp. 735-756, 1987.

[29] J. Drouet, L. Dupuy, F. Onimus and F. Mompiou, "A direct comparison between in-situ transmission electron microscopy observations and Dislocation Dynamics simulations of interaction between dislocation and irradiation induced loop in a zirconium alloy," *Scripta Materialia,* vol. 119, pp. 71-75, 2016.

[30] X. J. Shi, L. Dupuy, B. Devincre, D. Terentyev and L. Vincent, "Interaction of< 1 0 0> dislocation loops with dislocations studied by dislocation dynamics in α-iron.," *Journal of Nuclear Materials,* vol. 460, pp. 37-43, 2015.

[31] "PROJECT NUMODIS : Numerical Modelling of Dislocations," [Online]. Available: www.numodis.fr. [Accessed 17 06 2021].

[32] A. Stukowski, "Visualization and analysis of atomistic simulation data with OVITO–the Open Visualization Tool," *Modelling and Simulation in Materials Science and Engineering,* vol. 18, no. 1, p. 015012, 2009.

[33] J. D. Honeycutt and H. C. Andersen, "Molecular dynamics study of melting and freezing of small Lennard-Jones clusters," *Journal of Physical Chemistry,* vol. 91, no. 19, pp. 4950-4963, 1987.

[34] A. Stukowski and K. Albe, "Extracting dislocations and non-dislocation crystal defects from atomistic simulation data.," *Modelling and Simulation in Materials Science and Engineering,* vol. 18, no. 8, p. 085001, 2010.

[35] L. K. Béland, Y. N. Osetsky and R. E. Stoller, "Atomistic material behavior at extreme pressures.," *npj Computational Materials,* vol. 2, no. 1, pp. 1-4, 2016.

[36] H. Trinkaus, "Local stress relaxation in thermal spikes as a possible cause for creep and macroscopic stress relaxation of amorphous solids under irradiation.," *Journal of nuclear materials,* vol. 223, no. 2, pp. 196-201, 1995.

[37] V. P. Zhukov and A. A. Boldin, "Interaction of Cascade-Generated Nonlinear Elastic Waves with Dislocation Structure Elements in Metals.," *physica status solidi (b),* vol. 2, no. 339-346, p. 166, 1991.

[38] C. Borschel and C. Ronning, "Ion beam irradiation of nanostructures - A 3D Monte Carlo simulation code," *Nuclear Instruments and Methods in Physics Research Section B: Beam Interactions with Materials and Atoms ,* vol. 269, pp. 2133-2138 , 2011.

[39] J. P. Crocombette and C. Wambeke, "Quick calculation of damage for ion irradiation: implementation in Iradina and comparisons to SRIM.," *EPJ Nuclear Sci. Technol.,* vol. 5, 2019.

[40] A. De Backer, C. Domain, C. S. Becquart, L. Luneville, D. Simeone, A. E. Sand and K. Nordlund, "A model of defect cluster creation in fragmented cascades in metals based on morphological analysis.," *ournal of Physics: Condensed Matter,* vol. 30, no. 40, p. 405701, 2018.